Separation Science and Technology
Publication details, including instructions for authors and subscription information:
http://www.informaworld.com/smpp/title~content=t713708471

SANS Study of Third Phase Formation in the Extraction of HCl by TBP Isomers in *n*-Octane

R. Chiarizia[a]; D. C. Stepinski[a]; P. Thiyagarajan[b]
[a] Chemistry Division, Argonne National Laboratory, Argonne, IL, USA [b] IPNS Division, Argonne National Laboratory, Argonne, IL, USA

To cite this Article Chiarizia, R. , Stepinski, D. C. and Thiyagarajan, P.(2006) 'SANS Study of Third Phase Formation in the Extraction of HCl by TBP Isomers in *n*-Octane', Separation Science and Technology, 41: 10, 2075 — 2095
To link to this Article: DOI: 10.1080/01496390600742716
URL: http://dx.doi.org/10.1080/01496390600742716

Separation Science and Technology, 41: 2075–2095, 2006

ISSN 0149-6395 print/1520-5754 online
DOI: 10.1080/01496390600742716

SANS Study of Third Phase Formation in the Extraction of HCl by TBP Isomers in *n*-Octane

R. Chiarizia and D. C. Stepinski
Chemistry Division, Argonne National Laboratory, Argonne, IL, USA

P. Thiyagarajan
IPNS Division, Argonne National Laboratory, Argonne, IL, USA

Abstract: Third phase formation in the extraction of HCl by triisobutyl phosphate (T-*iso*-BP) and tri-*sec*-butyl phosphate (T-*sec*-BP) has been investigated and compared with the tri-*n*-butyl phosphate (T-*n*-BP) system. The three TBP isomers exhibit comparable affinities for HCl, but the branched isomers extract much more water than the linear one. For T-*sec*-BP, the LOC (limiting HCl organic concentration) is characterized by much lower HCl concentrations both in the organic and aqueous phase than for the other isomers. SANS data for T-*iso*-BP and T-*sec*-BP organic phases loaded with progressive amounts of HCl have been interpreted using the Baxter model for hard spheres with surface adhesion. The critical values of the stickiness parameter, τ^{-1}, and the interaction potential energy, U(r), are slightly different and characteristic for each of the extractants. Their values are consistent with the expectation derived from the micellar interaction model.

Keywords: TBP, HCl extraction, third phase formation

Received 25 October 2005, Accepted 1 February 2006

Address correspondence to R. Chiarizia, Chemistry Division, Argonne National Laboratory, Argonne, IL 60439, USA. Fax: 630-252-7501; E-mail: chiarizia@anl.gov

INTRODUCTION

Recent works have presented a new interpretation of third phase formation in solvent extraction, the generally unwanted phenomenon by which the organic phase, under certain conditions, splits into two liquid phases of different compositions and densities (1–9). These works have mostly focused on *n*-alkane solutions of tri-*n*-butyl phosphate (T-*n*-BP) as the extractant for HNO_3 (3–6), $UO_2(NO_3)_2$ (4, 6), $Th(NO_3)_4$ (5, 7), $Zr(NO_3)_4$ (8), and, very recently, HCl (9).

Small-angle X-ray (SAXS) (3) and neutron (SANS) (3–9) scattering measurements on T-*n*-BP solutions containing increasing concentrations of solutes (up to the point of phase splitting) were interpreted using the Baxter model for hard spheres with surface adhesion (sticky spheres) (10–12) to quantitatively evaluate the energetics of the interactions between small T-*n*-BP aggregates resembling reverse micelles.

In all systems investigated, the application of the Baxter model to the scattering data provided the following mechanistic explanation for third phase formation: the T-*n*-BP molecules, at high concentrations in *n*-alkanes, upon contact with aqueous phases containing mineral acids with or without metal salts, forms small reverse micelles containing only a few T-*n*-BP molecules, in agreement with previous anticipations by Osseo-Asare (13). Water and inorganic solutes are incorporated into the polar core of the micelles which interact through van der Waals forces between their polar cores. The separation of most of the solute particles in a new phase takes place when the energy of attraction between the particles in solution becomes at least about twice as large as the average thermal energy (k_BT, where k_B = Boltzmann constant). Most of the solutes from the original organic phase (T-*n*-BP, water, HNO_3 or HCl, and metal salts) collect in a separate and denser third phase containing interspersed layers or pockets of *n*-alkane.

The extraction of HCl alone proved to be particularly useful for this type of studies, because third phase formation could be easily observed in the absence of metal salts. In this way, the experimental burden of data acquisition and the difficulty of their interpretation were reduced (9). As part of our ongoing investigation on the general validity of the mechanism of third phase formation outlined above, we decided to use the extraction of HCl to probe the phase behavior of other solvent extraction systems.

Formation of micelles by neutral organophosphorus extractants and the properties of the hydrophobic shell of the micelles should be affected by the type of alkyl chains attached to the functional group of the extractant. In particular, it should be of interest to measure the impact of length and branching of the alkyl chains on the energy of interaction between micelles. In this paper, we focus on the branching of butyl chains of tributyl phosphate, by comparing the behavior of tri(2-methylpropyl) phosphate (also known as triisobutyl phosphate, T-*iso*-BP) and of tri(1-methylpropyl) phosphate (also known as

tri-*sec*-butyl phosphate, T-*sec*-BP) with that of T-*n*-BP reported earlier (9) (Fig. 1).

The behavior of the *iso* and *sec* TBP isomers is particularly interesting because they have been considered as potential alternatives to T-*n*-BP for nuclear applications. In fact, T-*iso*-BP offers the advantage of being about five times more stable to acid hydrolysis than T-*n*-BP (14). At the same time, the distribution ratios of U(VI) and Pu(IV) from nitric acid solutions are only slightly lower than with T-*n*-BP. This is probably the result of a balance between the somewhat higher basicity of the phosphoryl group of T-*iso*-BP and the steric hindrance caused by the branching of its alkyl chains (15). A drawback for the use of T-*iso*-BP in uranium purification processes, however, consists in its slightly higher tendency than T-*n*-BP toward third phase formation (15).

In spite of its considerably lower stability toward acid hydrolysis than T-*n*-BP (14), T-*sec*-BP has been considered for the selective extraction and separation of U(VI) from Th(IV). This separation is based on the drastic reduction of Th(IV) extraction brought about by the branching in the *sec*-butyl group (16). Regarding third phase formation, the T-*sec*-BP has been reported to exhibit less tendency than T-*n*-BP toward phase splitting (16).

The different behavior of the two TBP isomers with respect to third phase formation, with T-*iso*-BP being more effective and T-*sec*-BP less effective than T-*n*-BP in promoting organic phase splitting, is intriguing and so far

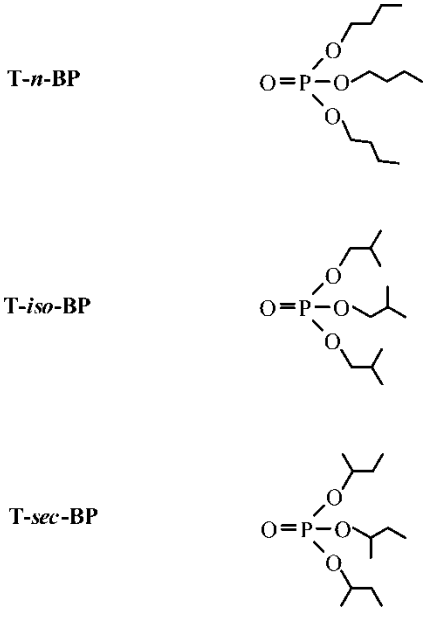

Figure 1. Structures of T-*n*-BP, T-*iso*-BP and T-*sec*-BP.

unexplained. The interpretation of third phase formation based on the Baxter model implies that the branched isomers of TBP should exhibit a higher tendency toward phase splitting than T-*n*-BP, because shorter alkyl chains should allow the extractant micelles to get closer to one another, thus experiencing a stronger attraction between their polar cores.

The present paper reports our results on the extraction of HCl by the *iso* and *sec* isomers of TBP with particular emphasis on third phase formation. The objectives of this work were:

- To measure the distribution isotherm of HCl and the simplified phase diagram for the T-*iso*-BP and T-*sec*-BP extractants in *n*-octane;
- To evaluate the morphology of the aggregates formed in the organic phase using SANS measurements;
- To determine whether the particle interaction model developed in our previous studies on T-*n*-BP extraction systems can explain the features of third phase formation with T-*iso*-BP and T-*sec*-BP.

EXPERIMENTAL

Materials

Triisobutyl phosphate was obtained from Fluka, Switzerland, as a >97% product. The purity of T-*iso*-BP was confirmed by ^{31}P and ^{1}H NMR analysis. Before the extraction experiments, the 20% (v/v) stock solution of the extractant in *n*-octane (0.73 M) was washed with an aqueous solution of 0.25 M Na_2CO_3 to remove any acidic impurities undetectable by NMR.

Tri-*sec*-butyl phosphate was prepared through the following procedure (17). A mixture of *sec*-butyl alcohol (48.7 mL, 0.531 mol) and pyridine (43.0 mL, 0.531 mol) in 100 mL of toluene was added dropwise over a 2 hr period to phosphorus oxychloride (15.0 mL, 0.161 mol) dissolved in 100 mL toluene. After overnight stirring at room temperature under a nitrogen atmosphere, the organic phase was washed with three 50 mL portions of 0.2 M HCl. Toluene was removed from the product mixture under reduced pressure in a rotary evaporator. The bulk of the acidic impurities was removed from a methanol solution of the product using a Bio-Rad AG 1-Xa, 50-100 mesh, chloride form ion exchange resin, as described previously (18). The final product was further purified by vacuum distillation. However, a small amount (< 5%) of diisobutyl phosphoric acid was still present in the product. Repeating the ion exchange or the distillation procedure did not improve significantly the purity of the product. This confirms that the tri-*sec*-butyl phosphate is more unstable than the other TBP isomers investigated (14).

After washing the tri-*sec*-butyl phosphate product with 0.25 M Na_2CO_3, ^{1}H NMR measurements indicated that the extractant contained 5% of

sec-butyl alcohol and 0.5 mole water per mole product. The 0.73 M stock solution of the extractant in *n*-octane for the extraction experiments was prepared based on these results. The possible effect of the presence of 5% of *sec*-butyl alcohol on third phase formation with T-*sec*-BP will be discussed in a following section.

The other materials used for the distribution measurements and for the preparation of the SANS samples were the same as in our previous works (4–9).

Solvent Extraction Experiments

The technique and analytical procedures used for the HCl extraction experiments were reported previously (9). Similarly to the T-*n*-BP case, the equilibration time for the aqueous and organic phases was kept to the minimum necessary for attaining distribution equilibrium (about ten minutes), because HCl is known to promote TBP hydrolysis much more efficiently than HNO_3 (19).

For the determination of the HCl limiting organic concentration (LOC, i.e., the highest acid concentration attainable in the organic phase without phase splitting), the initial aqueous concentration of HCl was high enough that a third phase formed. Very small amounts of fresh organic phase and water were then added to the system until the third phase disappeared, as indicated by the visual absence of turbidity in the organic phase after further equilibration and centrifugation.

To determine the extractant concentration in the heavy and light organic phases, HCl was stripped with water and the samples diluted to appropriate concentrations with *n*-octane. The distribution ratios (D_U) of freshly purified ^{233}U (from ANL stocks) between the organic phase samples and 3.0 M HNO_3 were then measured and the concentrations of T-*iso*-BP and T-*sec*-BP were determined using their respective D_U vs. extractant concentration calibration curves.

The samples for SANS measurements were prepared as described above except that the diluent used was deuterated *n*-octane (D-octane, in the following). Their composition is summarized in Table 1.

SANS Measurements

The SANS measurements were performed at the time-of-flight small-angle neutron diffractometer (SAND) at the Intense Pulsed Neutron Source of Argonne National Laboratory (21). The samples were measured in standard Suprasil cells with a pathlength of 2 mm and a sample volume of 0.8 mL. The data collection time was four hours. For each sample the data were collected as scattered intensity, I(Q) (cm^{-1}) vs momentum transfer

Table 1. Composition of samples for SANS measurements (T = 23 ± 0.5°C)

Sample	[TBP][a] M	[HCl][b] M	[H_2O][c] M	η[d]
T-*iso*-BP				
blank1	0.73	0	0.128	0.204 ± 0.004
1	0.73	0.0856	0.35	0.209 ± 0.004
2	0.73	0.172	0.57	0.215 ± 0.004
3	0.73	0.283	0.74	0.220 ± 0.004
4 (LOC)[e]	0.73	0.313	0.75	0.221 ± 0.004
5 (Third phase)[f]	2.35	2.58	5.21	0.79 ± 0.03
6 (Light phase)[f]	0.31	0.15	0.18	0.092 ± 0.003
T-*sec*-BP				
blank2	0.73	0	0.061	0.188 ± 0.004
7	0.73	0.0268	0.26	0.192 ± 0.004
8	0.73	0.0625	0.43	0.195 ± 0.004
9 (LOC)[e]	0.73	0.141	0.68	0.201 ± 0.004
10 (Third phase)[g]	2.31	2.71	11.0	0.84 ± 0.03
11 (Light phase)[g]	0.20	0.0603	0.035	0.053 ± 0.002

[a]Estimated accuracy ± 2%, except for third and light phase samples for which the estimated accuracy is ± 5%.

[b]Estimated accuracy ± 2%.

[c]Estimated accuracy ± 10%.

[d]Solute volume fraction given by the sum of T-*iso*-BP or T-*sec*-BP, HCl, and H_2O volume fractions. The molar volumes (ratio of molecular weight and density) of the components are 275.98, 255.34, 18.50, and 18.02 cm^3, respectively. The molar volume of HCl was calculated from the density of dilute solutions of the acid (20). The uncertainty on η was estimated from the errors associated with the analytical determinations.

[e]LOC stands for limiting organic concentration, i.e., the highest HCl concentration that can be achieved without phase splitting.

[f]Initial conditions: 3.0 mL 0.73 M T-*iso*-BP in *n*-octane equilibrated with 3.0 mL 10.34 M HCl. After centrifugation, the volumes of the organic phases were 0.65 mL third phase with a density of 0.931 g/mL (sample 5), and 2.35 mL light phase with a density of 0.722 g/mL (sample 6).

[g]Initial conditions: 2.2 mL 0.73 M T-*sec*-BP in *n*-octane equilibrated with 2.2 mL 8.55 M HCl. After centrifugation, the volumes of the organic phases were 0.60 mL third phase with a density of 1.00 g/mL (sample 10), and 1.70 mL light phase with a density of 0.702 g/mL (sample 11).

($Q = (4\pi/\lambda)\sin(\theta)$ ($Å^{-1}$)), where θ is half the scattering angle and λ is the wavelength of the probing neutrons. In our experiments, the contrast between solute and solvent was given by the different neutron scattering properties of the H atoms of TBP and the D atoms of deuterated *n*-octane.

The absolute intensity of the scattering data at $Q = 0$ was obtained using as secondary standards polymer and porous silica samples with known cross sections, following the procedure reported previously (22).

Calculations

The equation describing neutron scattering by a monodisperse system of particles is:

$$I(Q) = N_p V_p^2 (\rho_p - \rho_s)^2 P(Q) S(Q) + I_{inc} \quad (1)$$

where I(Q) is the intensity of the neutrons scattered by the solute particles (obtained from the experimental intensities by subtracting the intensities measured for the diluent alone), N_p is the number of scattering units per unit volume, V_p is the particle volume, ρ_p and ρ_s are the scattering length densities of particles and solvent, respectively, P(Q) is the single particle form factor, which describes the angular scattering distribution as a function of particle size and shape, S(Q) is the structure factor, which accounts for interactions between the scattering particles, and I_{inc} is the incoherent scattering background (23).

Guinier analysis and modified Guinier analysis for rod-like particles (24) were performed on the SANS data using the procedures and equations reported previously (9).

The evaluation of the extent of interaction between particles was performed using the Baxter model following the procedure described previously (5–9). According to this model, an approximate value of the potential energy of attraction (negative) between two hard spheres, U(r), expressed in k_BT units, is given by the following equation:

$$U(r) = \lim_{\delta \to d_{hs}} \ln\left[12\tau\left(\frac{\delta - d_{hs}}{d_{hs}}\right)\right] \quad (2)$$

where d_{hs} is the diameter of the hard spheres and (δ-d_{hs}) represents the width of a narrow square attractive well. When the distance between two particles is larger than d_{hs} but smaller than δ (i.e., for $d_{hs} < r < \delta$), the particles experience attraction. Use of Eq. (2) requires knowledge of the parameterτ. τ^{-1}, also expressed in k_BT units, is the "stickiness parameter" and its value is higher for stronger attraction between particles. The limit in Eq. (2) indicates that the calculation of the interparticle attraction potential energy is valid only when the attractive well is extremely narrow, i.e., with a width within 10% of the particle diameter ((δ - d_{hs}) / $d_{hs} \leq 0.1$). The Baxter model provides analytical expressions for the structure factor, S(Q), in Eq. (1). They have been reported earlier (2, 10–12). Other details of the Baxter model calculations for the SANS data of this paper will be discussed in one of the following sections.

RESULTS AND DISCUSSION

HCl Extraction by T-*iso*-BP and T-*sec*-BP

Figure 2 shows the simplified phase diagrams for the extraction of HCl by 0.73 M T-*iso*-BP and T-*sec*-BP in *n*-octane and compares them with the results for T-*n*-BP reported earlier (9). The points corresponding to the HCl limiting organic concentration (LOC) are identified by the intersection of the three curves describing the organic HCl concentrations in the biphasic and triphasic regions of the diagrams. The organic phase splits into two layers when the equilibrium concentration of HCl in the aqueous phase is higher than that corresponding to the LOC condition for that particular system.

As can be seen in the biphasic regions of the plots in Fig. 2, the extractability of HCl by T-*n*-Bp and T-*iso*-BP is about the same, while T-*sec*-BP is somewhat more efficient than the other two isomers. This is likely the result of the interplays between the enhanced basicity of the TBP isomers having branched alkyl chains and the steric effects due to branching.

As shown in Table 1 and already reported for T-*n*-BP (9), the concentrations of the TBP isomers in the heavy layer are as high as 2.3 M. The concomitant HCl concentrations (see Table 1) indicate that the third phases can be considered as concentrated solutions of the respective HCl hydrated monosolvates, in agreement with literature information available for T-*n*-BP (9, 25).

As for the T-*n*-BP case, the data in Table 1 confirm that the extraction of HCl by the TBP isomers is accompanied by simultaneous extraction of large amounts of water. The water to acid concentration ratios in the LOC samples for the *iso* and *sec* isomers, however, are 2.4 and 4.8, respectively, i.e., substantially higher than for T-*n*-BP (9). In the third phase samples, the concentration of water is twice that of HCl for T-*iso*-BP, and four times that of HCl for T-*sec*-BP, confirming the pronounced hydration of the HCl-TBP monosolvates (25).

Regarding third phase formation, although the general behavior of the three isomers is similar, two major differences can be seen in Fig. 2. First, the aqueous HCl concentrations where organic phase splitting occurs change into opposite directions for the *iso* and *sec* isomers as compared with T-*n*-BP (compare 7.3 M for T-*n*-BP with 8.0 M for T-*iso*-BP and 5.9 M for T-*sec*-BP). Second, the actual HCl LOC values are the same within experimental uncertainties for T-*n*-BP and T-*iso*-BP, but the LOC for T-*sec*-BP is considerably lower (compare 0.31 M for T-*n*-BP and T-*iso*-BP with 0.14 M for T-*sec*-BP). This is in sharp contrast to previous results which show that, for the extraction of Th(IV) from HNO_3 solutions, T-*iso*-BP in *n*-dodecane is less prone to third phase formation than T-*n*-BP, while for T-*sec*-BP the opposite is true (15, 16). However, comparisons between TBP third phase formation under different aqueous phase conditions (nitrate vs. chloride systems) may be misleading given the vastly different behavior of water in the two cases, with very little water being extracted into the organic phase from nitric acid aqueous media (25, 26).

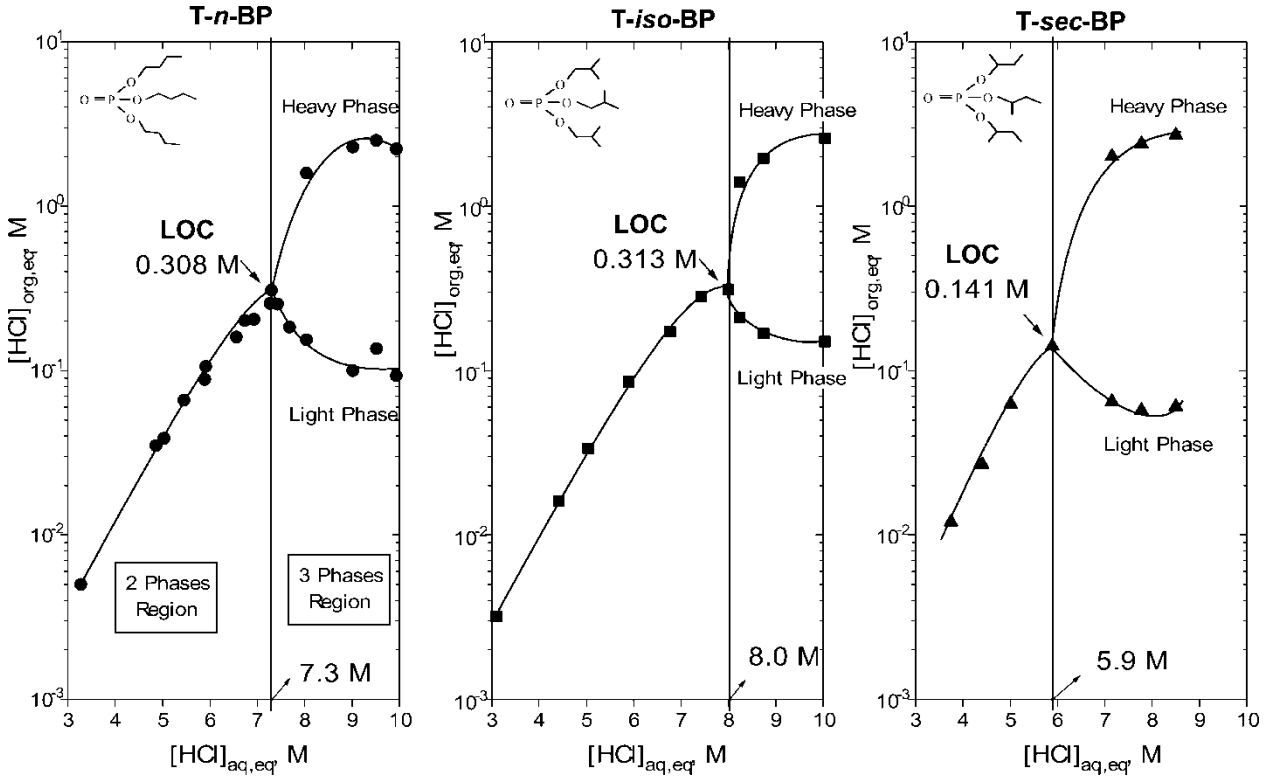

Figure 2. Distribution isotherm and simplified phase diagram for the extraction of HCl by 0.73 M T-*n*-BP, T-*iso*-BP and T-*sec*-BP in *n*-octane at 23 $\pm$ 1°C. (Data for T-*n*-BP taken from reference 9).

As reported in a previous section, the T-*sec*-TBP extractant used in this study contained about 5% of *sec*-butyl alcohol. The presence of this impurity cannot be responsible for the lower LOC coordinates observed for this isomer in Fig. 2 as compared to the other isomers. Alcohols, in fact, act as solvent modifiers and typically shift the critical point of third phase formation toward higher LOC and aqueous equilibrium solute concentrations (27). Without the alcohol impurity, the LOC coordinates for T-*sec*-BP in Fig. 2 would be even lower.

SANS Data

Figure 3 (experimental points) shows the SANS data for most of the organic phase samples in Table 1.

The data in Fig. 3 clearly show how the scattering intensity in the low Q region increases when increasing amounts of HCl, up to the LOC condition, are extracted by the *iso* and *sec* TBP isomers. After phase splitting, much lower intensities are exhibited for both systems by the third phase and especially by the light phase samples (data shown in Fig. 4). The behavior of the TBP isomers strongly parallels that reported T-*n*-BP (9).

Table 2 reports the results of the Guinier analysis (ln[I(Q)] vs. Q^2) and modified Guinier analysis (ln[QxI(Q)] vs. Q^2) for cylindrical particles. These analyses were performed on the samples of Fig. 3 using the same assumptions, procedure and equations reported previously (9). For comparison, Table 2 also reports the results for the T-*n*-BP LOC sample (9).

The Guinier analysis provided the radius of gyration, R_g, and the scattering intensity at zero Q, I(0). The value of I(0) was used to calculate the weight-average aggregation number, n_w, of the extractant using the previously derived equation (28, 29):

$$n_w = \frac{M_w}{MW_{TBP}} = \frac{6.022 \times 10^{26} d_{TBP}^2 I(0)}{[TBP]_{total}(\rho_p - \rho_s)^2 MW_{TBP}^2} \quad (3)$$

In Eq. (3), M_w is the weight-average molecular weight of the extractant aggregates, MW_{TBP} and d_{TBP} are the molecular weight (266.32) and the densities of T-*iso*-BP and T-*sec*-BP (0.965 and 1.043 g/mL, respectively), and $[TBP]_{total}$ is the total extractant concentration in the organic phase. For the calculation of the contrast factor $(\rho_p - \rho_s)^2$, the following values were used for the scattering length densities: $\rho_p = 1.553 \times 10^9$ cm^{-2} for T-*iso*-BP and 1.679×10^9 cm^{-2} for T-*sec*-BP; $\rho_s = 6.426 \times 10^{10}$ cm^{-2} for D-octane. These ρ_p and ρ_s values were calculated from the scattering lengths of the individual atoms and the densities of the compounds.

The results in Table 2, obtained under the simplifying assumption that the increase in scattering observed at low Q is due only to an increase in size of

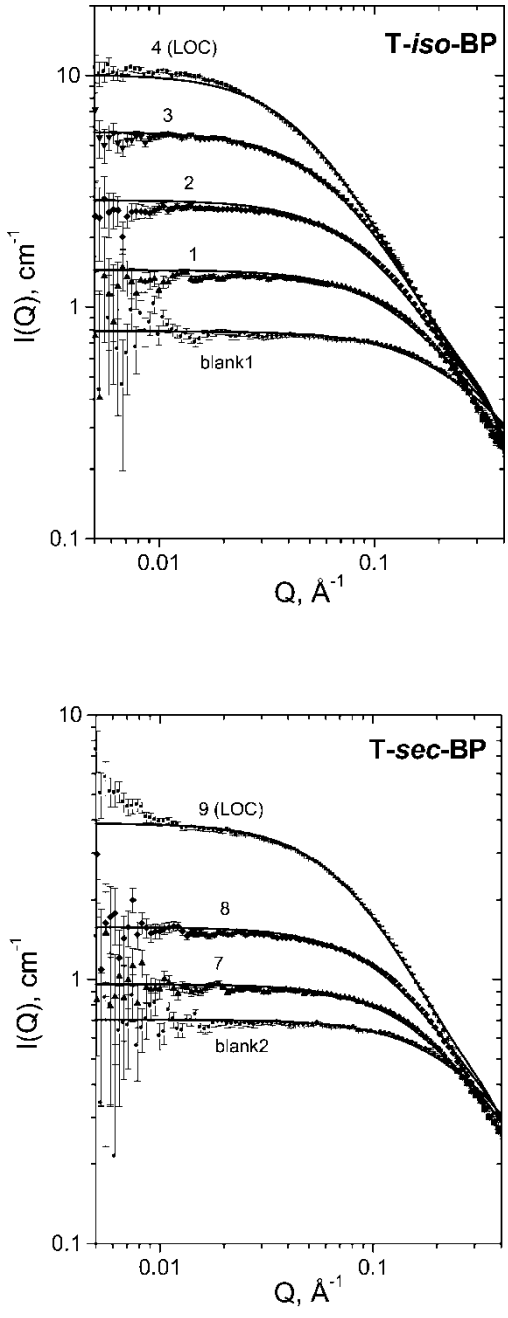

Figure 3. SANS data for T-*iso*-BP samples blank1 through 4(LOC) (upper panel), and for T-*sec*-BP samples blank2 through 9(LOC) (lower panel). The continuous lines were calculated using the Baxter model and the fit parameters reported in Table 3.

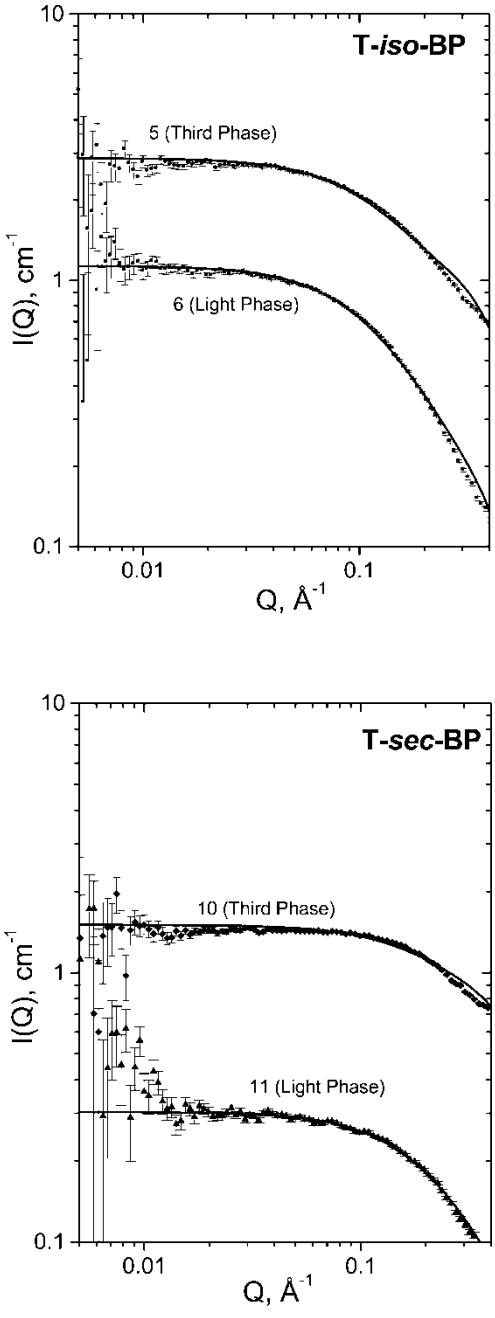

Figure 4. SANS data for T-*iso*-BP samples 5 and 6 (upper panel), and for T-*sec*-BP samples 10 and 11 (lower panel). The continuous lines were calculated using the Baxter model and the fit parameters reported in Table 3.

Table 2. Results from Guinier analysis and modified guinier analysis for cylindrical particles

Sample	R_g [a,b],Å	n_w [c,b]	R_{cyl} [d,e],Å	L [f,e],Å
T-*n*-BP				
LOC[g]	47 ± 2	54 ± 3	11.4 ± 0.6	183 ± 12
T-*iso*-BP				
Blank1	5.1 ± 0.1	2.0 ± 0.1	/	/
1	8.3 ± 0.1	3.6 ± 0.2	2.9 ± 0.1	31 ± 1
2	13.2 ± 0.3	7.2 ± 0.4	4.8 ± 0.1	47 ± 1
3	22 ± 1	15 ± 1	6.1 ± 0.1	77 ± 1
4 (LOC)	35 ± 3	29 ± 2	8.1 ± 0.1	125 ± 2
T-*sec*-BP				
Blank2	4.6 ± 0.1	2.2 ± 0.1	/	/
7	6.6 ± 0.1	2.8 ± 0.2	1.6 ± 0.1	25 ± 1
8	9.3 ± 0.2	4.6 ± 0.3	2.7 ± 0.1	34 ± 1
9 (LOC)	18 ± 1	11 ± 0.7	5.0 ± 0.1	64 ± 1

[a]Radius of gyration;
[b]From Guinier analysis;
[c]Weight-average extractant aggregation number;
[d]Radius of cylindrical micelles;
[e]From modified Guinier analysis for cylindrical particles;
[g]Length of cylindrical micelles;
[f]From reference 9.

non-interacting aggregates ($S(Q) = 1$ in Eq. (1)), indicate that the SANS data can be formally interpreted as resulting from the formation of large cylindrical micelles with lengths between 183 Å for the LOC sample of T-*n*-BP and 64 Å for that of T-*sec*-BP.

The trend in the R_g, n_w, R_{cyl} and L values for the LOC samples of the three TBP isomers in Table 2 is consistent with expectations. Shorter and branched alkyl chains should originate smaller, less aggregated and thinner cylindrical micelles. However, as previously reported for the other TBP extraction systems investigated (5–9), the existence in solution of large TBP aggregates is unlikely because reverse micelles typically have very small aggregation numbers (30). The scattering increase observed in the low Q range in Fig. 3 is more likely the result of critical concentration fluctuations due to interactions between small reverse micelles and to structure factors higher than unity ($S(Q) > 1$ in Eq. (1)).

For a quantitative evaluation of the interaction between micelles, Eq.(1) was used after introducing the expression for the solute volume fractions (see Table 1):

$$\eta = N_p V_p \tag{4}$$

Table 3. Results from Baxter model calculations

Sample	d_{hs} Å	n_w	Core diameter Å	Shell thickness Å	τ^{-1} k_BT	U(r) k_BT
T-*n*-BP						
LOC[a]	18.6 ± 0.2	7.0 ± 0.2	7.1 ± 0.2	5.8 ± 0.3	9.21 ± 0.04	−2.04 ± 0.01
T-*iso*-BP						
Blank1	12.9 ± 0.1	2.4 ± 0.1	2.9 ± 0.1	5.0 ± 0.1	3.95 ± 0.08	−1.19 ± 0.02
1	14.5 ± 0.1	3.3 ± 0.1	4.8 ± 0.1	4.8 ± 0.1	5.25 ± 0.08	−1.48 ± 0.02
2	16.2 ± 0.1	4.5 ± 0.1	6.4 ± 0.1	4.9 ± 0.1	6.47 ± 0.08	−1.69 ± 0.01
3	17.6 ± 0.1	5.7 ± 0.1	7.7 ± 0.1	4.9 ± 0.1	7.58 ± 0.06	−1.84 ± 0.01
4 (LOC)	17.9 ± 0.1	6.0 ± 0.1	7.9 ± 0.1	5.0 ± 0.1	8.62 ± 0.07	−1.97 ± 0.01
5 (Third phase)	18.2 ± 0.1	11.8 ± 0.2[b]	/	/	4.91 ± 0.07	−1.41 ± 0.02
6 (Light phase)	15.0 ± 0.2	3.6 ± 0.2	6.1 ± 0.2	4.5 ± 0.3	7.19 ± 0.05	−1.79 ± 0.01
T-*sec*-BP						
Blank 2	12.9 ± 0.1	2.7 ± 0.1	2.3 ± 0.1	5.3 ± 0.1	3.58 ± 0.06	−1.09 ± 0.02
7	13.3 ± 0.1	2.8 ± 0.1	4.0 ± 0.1	4.7 ± 0.1	4.60 ± 0.06	−1.34 ± 0.01
8	14.4 ± 0.1	3.5 ± 0.1	5.2 ± 0.1	4.6 ± 0.1	5.59 ± 0.06	−1.54 ± 0.01
9 (LOC)	15.9 ± 0.1	4.6 ± 0.1	6.7 ± 0.1	4.6 ± 0.1	7.34 ± 0.05	−1.81 ± 0.01
10 (Third phase)	12.8 ± 0.2	7.0 ± 0.2[b]	/	/	3.42 ± 0.11	−1.05 ± 0.03
11 (Light phase)	15.3 ± 0.1	2.5 ± 0.2	4.1 ± 0.2	4.3 ± 0.3	6.16 ± 0.15	−1.64 ± 0.03

[a]From reference 9;

[b]The n_w values for sample 5 and 10 represent the number of *n*-octane molecules contained in pockets or layers of diluent interspersed in the third phases.

P(Q) in Eq. (1) was calculated using the form factor of a sphere having a diameter equal to d_{hs} (31), while S(Q) was calculated using the equations reported previously (2, 10–12).

The three parameters I_{inc}, d_{hs} and τ were used as fit parameters and were optimized as described previously (5–9). The nonlinear curve fitting features of the Origin™ program (Microcal™ Software, Inc.) provided the uncertainty associated with the fit parameters. The continuous lines in Figs. 3 and 4 show the Baxter model fit of the SANS data. The data for the third phase samples were fitted using the procedure described previously (5–9), which assumes that the third phase samples are continuous phases made of extractant, HCl, water and interspersed small amounts of *n*-octane. Table 3 summarizes the values of the diameter of the hard sphere, d_{hs}, and of the stickiness parameter, τ^{-1}, provided by the Baxter model calculations. The values of the parameters reported previously for the T-*n*-BP LOC sample (9) are included in Table 3 for comparison.

The values of the hard sphere diameter, d_{hs}, obtained for each sample from the Baxter model fit of the SANS data, were used to calculate the volume of the spherical scattering particles. This volume comprises both the volume of the inorganic constituents of the micelle (the polar core) and the volume occupied by the extractant (the lipophilic shell). By using the analytical data in Table 1, the volume of the shell was estimated by subtracting from V_p the volume occupied by the inorganic solutes. Finally, the weight-average aggregation number of the extractant in the micelle, n_w, was calculated by dividing the volume of the shell by the molecular volume of the TBP isomers (4.58×10^{-22} cm^3 for T-*iso*-BP and 4.24×10^{-22} cm^3 for T-*sec*-BP), while the thickness of the shell was obtained from d_{hs} and the diameter of the core. Table 3 also includes the n_w values (for the third phase samples, however, n_w represents the number of *n*-octane molecules contained in pockets or layers interspersed in the third phase).

From the τ values, the attractive potential energy between two particles, U(r) in k_BT units, was calculated through Eq. (2), assuming a width of the attractive well equal to 10% of the hard sphere diameter. The U(r) values are also reported in Table 3 together with the diameter of the inorganic core and the shell thickness.

The d_{hs}, n_w and core diameters values for T-*iso*-BP and T-*sec*-BP in Table 3 are consistent with the HCl extraction mechanism proposed earlier for T-*n*-BP(9). In the absence of inorganic solutes, the TBP isomers exists in solution as dimeric species. Upon extraction of HCl and water, the extractant molecules organize in the form of small reverse micelles that swell when more HCl and water report into their polar core. The swelling, clearly documented by the large increase of the values of the core diameters in Table 3, creates the spatial conditions for accommodating more TBP molecules into the hydrophobic shell of the micelles. The values of n_w for the LOC samples change from 7 (T-*n*-BP) to 6 (T-*iso*-BP), to 5 (T-*sec*-BP). This trend reflects the steric hindrance due to branching, especially on the first carbon atom.

Without accounting for the core swelling, the hard sphere diameters for the T-*iso*-BP and T-*sec*-BP LOC samples should be about 2.5 Å shorter than for T-*n*-BP (the projection along the direction of the alkyl chain of a C-C bond length (1.54 Å) with a C-C-C bond angle of 109.5° is equal to 1.26 Å(30)). Overall the d_{hs} values for the T-*iso*-BP and T-*sec*-BP LOC samples are indeed shorter than for T-*n*-BP, but less than predicted based on the length of a propyl vs. a butyl chain, because of the more pronounced swelling of the micellar core due to enhanced water extraction by the *iso* and *sec* isomers.

The length of a fully extended hydrocarbon tail with n carbon atoms attached to the polar group of a surfactant, l_{max}, can be calculated with the help of Tanford's equation (30):

$$l_{max} = (1.5 + 1.265n)\text{Å} \quad (5)$$

For n equal to four or three, Eq. (5) provides a maximum length of 6.6 Å and 5.3 Å for the butyl and propyl chains of T-*n*-BP and the branched isomers, respectively. The values of the shell thickness for the LOC samples in Table 3 (5.8, 5.0 and 4.6 Å, for T-*n*-BP, T-*iso*-BP and T-*sec*-BP), are within 87% and 94% of the maximum lengths of the respective chain lengths. It is generally expected that the effective length of a hydrocarbon tail in the liquid state is within 80% of its fully extended chain length (30, 32).

Based on the analytical results in Table 1, at the LOC condition, each T-*iso*-BP micelle should contain six molecules of extractant plus three molecules of HCl and six molecules of water. Similarly, the LOC micelle of T-*sec*-BP should include five molecules of extractant and one and five molecules of acid and water, respectively. By using the values of the core diameters and shell thicknesses in Table 3, the micelles present in the LOC samples can be schematically represented as shown in Fig. 5.

Regarding the energetics of third formation in the extraction systems investigated in this work, it remains to discuss whether the results in Table 3 are consistent with the expectations derived from our micellar interaction model. Both the values of the stickiness parameter, τ^{-1}, and the interaction energy, U(r), for the three TBP isomers indicate that at the point of phase splitting (LOC condition) the micelles interact progressively less strongly in moving from T-*n*-BP to T-*iso*-BP and T-*sec*-BP. At first sight this seems to contradict the concept that micelles with a thinner hydrophobic shell should experience more strongly the van der Waals attraction between their polar cores. However, the trends exhibited by the τ^{-1} and U(r) values in Table 3 can be rationalized when the structure of the alkyl chains of the three extractants is properly taken into account.

The merging of the reverse micelles into a new phase is equivalent to a process of micelle fusion. For this to happen, the micelles must co-penetrate and loose their individuality. The fusion of two micelles is more difficult and requires a higher energy of interaction for longer chains (T-*n*-BP). For

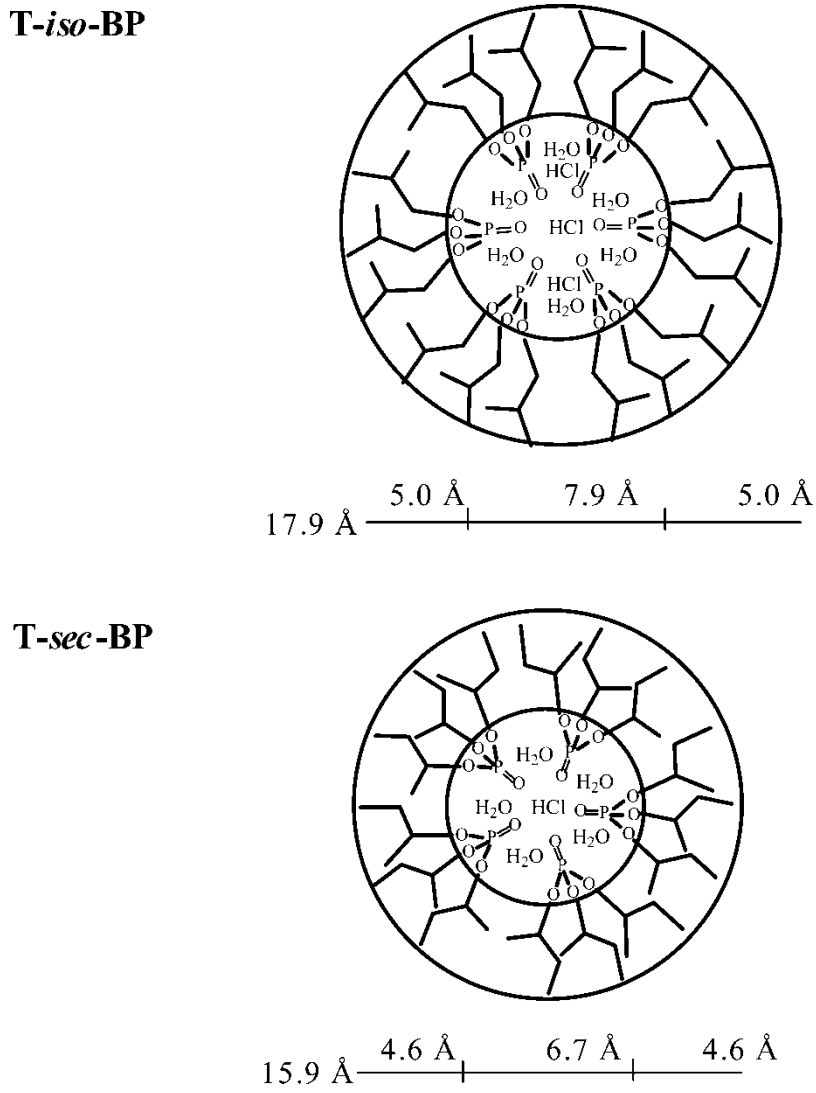

Figure 5. Schematic two-dimensional representation of the T-*iso*-BP and T-*sec*-BP reverse micelles for samples 4 (LOC) and 9 (LOC).

shorter chains with branching at the far end (T-*iso*-BP) the fusion is still relatively difficult because of the steric micellar stabilization provided by the branching (micellar fusion is hampered by far end branching). The fusion process is easier and therefore takes place at a lower attraction energy when the alkyl chains are shorter and the branching is closer to the micellar core (T-*sec*-BP).

These considerations should reflect in how rapidly the intermicellar energy of attraction increases as a function of the HCl concentration in the organic phase, i.e., in the value of the derivative $d(U(r))/d[HCl]_{org}$. This value for the three extractants can be estimated from the data in Fig. 6, where $-U(r)$ is plotted vs. $[HCl]_{org}$.

Figure 6 shows that the attraction energy increases more rapidly with $[HCl]_{org}$ when the alkyl chain is shorter because the dipole-dipole attraction is felt more strongly over a shorter distance. This effect is less evident for T-*iso*-BP because the terminal branching prevents the two micelles from merging easily. The terminal branching, thus, provides a sterical stabilization that can be overcome only by a stronger energy of attraction. The lower U(r) value observed for T-*sec*-BP is an indication that with this extractant the merging of the micelles into a separate phase is easier and the critical U(r) is reached more rapidly and at lower concentration of HCl in the organic phase than with the other two extractants.

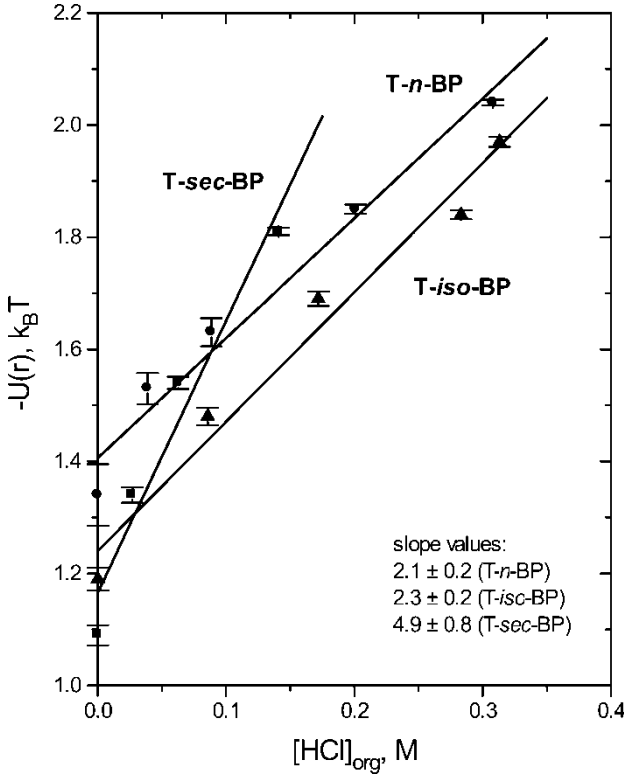

Figure 6. Plot of $-U(r)$ vs. $[HCL]_{org}$ for T-*n*-BP, T-*iso*-BP and T-*sec*-BP. (Data for T-*n*-BP taken from reference 9).

CONCLUSIONS

Measurements of the distribution of HCl and H_2O between aqueous solutions and *n*-octane solutions of three TBP isomers, T-*n*-BP, T-*iso*-BP and T-*sec*-BP, have shown that the three extractants exhibit comparable affinities for HCl. However, the branched isomers extract much more water than the linear one.

The point of third phase formation is reached by T-*iso*-BP at a slightly higher HCl aqueous concentration than for T-*n*-BP. The opposite is true for T-*sec*-BP, for which the LOC condition is characterized by much lower HCl concentrations both in the organic and aqueous phase.

SANS data for samples of T-*iso*-BP and T-*sec*-BP organic phases loaded with progressive amounts of HCl and water up to the LOC condition were interpreted using the same mechanism reported earlier for T-*n*-BP (9), with the help of the Baxter model for hard spheres with surface adhesion. This model analyzes the features of the scattering data in the low Q region as arising from van der Waals interactions between the polar cores of reverse micelles. The extractant micelles swell when more HCl and water are extracted into their polar core and reach a maximum TBP aggregation number of six for T-*iso*-BP and five for T-*sec*-BP. For these two extractants the diameters of the micelles at the LOC conditions are 18 and 16 Å, respectively, with shell thicknesses within about 90% of the length of the fully extended alkyl chains.

The critical values of τ^{-1} and U(r) are slightly different and characteristic for each of the extractants, depending on both the length and the branching of the alkyl chains. In the case of T-*sec*-BP, the shorter alkyl chains with branching close to the micellar core require a significantly lower energy of attraction than with the other isomers for the reverse micelles to merge into a separate third phase.

ACKNOWLEDGMENTS

We thank the personnel of the Analytical Chemistry Division of ANL for the water analyses and Denis Wozniak (IPNS) for help provided during the SANS measurements. This work was funded by the U. S. Department of Energy, Office of Basic Energy Science, Division of Chemical Sciences, Biosciences, and Geosciences (for the part performed at the Chemistry Division of ANL) and Division of Material Science (for the part performed at IPNS). The submitted manuscript has been created by the University of Chicago as Operator of Argonne National Laboratory ("Argonne") under Contract No. W-31-109-ENG-38 with the U.S. Department of Energy. The U.S. Government retains for itself, and others acting on its behalf, a paid-up, nonexclusive, irrevocable worldwide license in said article to reproduce, prepare derivative works, distribute copies to the public, and perform publicly and display publicly, by or on behalf of the Government.

REFERENCES

1. Erlinger, C., Gazeau, D., Zemb, Th., Madic, C., Lefrançois, L., Hebrant, M., and Tondre, C. (1998) Effect of nitric acid extraction on phase behavior, microstructure and interactions between primary aggregates in the system dimethyldibutyltetradecylmalonamide (DMDBTDMA)/n-dodecane/water. A phase analysis and small-angle x-ray scattering (SAXS) characterisation study. *Solvent Extr. Ion Exch.*, 16: 707–738.
2. Erlinger, C., Belloni, L., Zemb, Th., and Madic, C. (1999) Attractive interactions between reverse aggregates and phase separation in concentrated malonamide extractant solutions. *Langmuir*, 15: 2290–2300.
3. Nave, A., Mandin, C., Martinet, L., Berthon, L., Testard, F., Madic, C., and Zemb, Th. (2004) Supramolecular organization of tri-n-butyl phosphate in organic diluenton approaching third phase transition. *Phys. Chem. Chem. Phys.*, 6: 799–808.
4. Chiarizia, R., Jensen, M.P., Borkowski, M., Ferraro, J.R., Thiyagarajan, P., and Littrell, K.C. (2003) Third phase revisited: the U(VI), HNO_3–TBP, n-dodecane system. *Solvent. Extr. Ion Exch.*, 21: 1–27.
5. Chiarizia, R., Thiyagarajan, P., Jensen, M.P., Borkowski, M., and Littrell, K.C. (2003) Third phase formation in TBP solvent extraction systems as a result of interaction between reverse micelles. In *Proceedings of Hydrometallurgy*; Young, C.A., Alfantazi, A.M., Anderson, C.G., Dreisinger, D.B., Harris, B., and James, A. (eds.); The Minerals, Metals and Materials Society: Warrendale, PA; Vol. 1, Leaching and Solution Purification, 2003, 917–928.
6. Chiarizia, R., Nash, K.L., Jensen, M.P., Thiyagarajan, P., and Littrell, K.C. (2003) Application of the Baxter model for hard-spheres with surface adhesion to SANS data for the U(VI)-HNO_3, TBP-*n*-dodecane system. *Langmuir*, 19: 9592–9599.
7. Chiarizia, R., Jensen, M.P., Borkowski, M., Thiyagarajan, P., and Littrell, K.C. (2004) Interpretation of third phase formation in the Th(IV)-HNO_3, TBP-*n*-octane system with Baxter's "sticky spheres" model. *Solvent Extr. Ion Exch.*, 22: 1–27.
8. Chiarizia, R., Jensen, M.P., Rickert, P.G., Kolarik, Z., Borkowski, M., and Thiyagarajan, P. (2004) Extraction of zirconium nitrate by TBP in *n*-octane: influence of cation type on third phase formation according to the "Sticky Spheres" model. *Langmuir*, 20: 10798–10808.
9. Chiarizia, R., Rickert, P.G., Stepinski, D., Thiyagarajan, P., and Littrell, K.C. (2006) SANS study of third phase formation in the HCl-TBP-*n*-octane system. *Solvent Extr. Ion Exch.*, in press.
10. Baxter, R.J. (1968) Percus-Yevick equation for hard spheres with surface adhesion. *J. Chem. Phys.*, 49: 2770–2774.
11. Menon, S.V.G., Kelkar, V.K., and Manohar, C. (1991) Application of Baxter's model to the theory of cloud points of nonionic surfactant solutions. *Phys. Rev. A*, 43: 1130–1133.
12. Goyal, P.S., Menon, S.V.G., Dasannacharya, B.A., and Thiyagarajan, P. (1995) Small-angle neutron scattering study of micellar structure and interparticle interactions in Triton X-100 solutions. *Phys. Rev. E*, 51: 2308–2315.
13. Osseo-Asare, K. (1991) Aggregation, reversed micelles and microemulsions in liquid-liquid extraction: The tri-*n*-butyl phosphate–diluent–water–electrolyte system. *Adv. Colloid Interface Sci.*, 37: 123–173 (and references therein).
14. Yakshin, V.V., Filippov, E.A., Sokal'skaya, L.I., Serebryakov, I.S., and Dakalova, T.S. (1977) Study of the comparative hydrolytic stability of

isomeric tributyl phosphates in nitric acid solutions. *Radiokhimiya*, 19: 775–779.
15. Suresh, A., Srinivasan, T.G., and Vasudeva Rao, P.R. (1994) Extraction of U(VI), Pu(IV) and Th(IV) by some trialkyl phosphates. *Solvent Extr. Ion Exch.*, 12: 727–744.
16. Suresh, A., Subramaniam, S., Srinivasan, T.G., and Vasudeva Rao, P.R. (1995) Studies on U-Th separations using tri-*sec*-butyl phosphate. *Solvent Extr. Ion Exch.*, 13: 415–430.
17. Noller, C.R. and Dutton, G.R. (1933) Note on the preparation of trialkyl phosphates and their use as alkylating agents. *J. Am. Chem. Soc.*, 55: 424–425.
18. Zalupski, P.R., McAlister, D.R., Stepinski, D.C., and Herlinger, A.W. (2003) Metal extraction by silyl-substituted diphosphonic acids. III. Ester group substituent effects on phosphoryl oxygen basicity. *Solvent Extr. Ion Exch.*, 21: 331–345.
19. Kertes, A.S. and Halpern, M. (1961) Hydrochloric acid promoted hydrolysis of tri-*n*-butyl phosphate. *J. Inorg. Nucl. Chem.*, 20: 117–126.
20. Weast, R.C., Editor-in-Chief, *Handbook of Chemistry and Physics*; CRC Press, Inc: Boca Raton, FL, 1983–1984, D-236.
21. Thiyagarajan, P., Urban, V., Littrell, K.C., Ku, C., Wozniak, D.G., Belch, H., Vitt, R., Toeller, J., Leach, D., Haumann, J.R., Ostrowski, G.E., Donley, L.I., Hammonds, J., Carpenter, J.M., and Crawford, R.K. (1998) The performance of the small-angle diffractometer SAND at IPNS. In *ICANS XIV, The Fourteenth Meeting of the International Collaboration on Advanced Neutron Sources*; Starved Rock Lodge: Utica, IL; Vol. 2, June 14–19, 864–878.
22. Thiyagarajan, P., Epperson, J.E., Crawford, R.K., Carpenter, J.M., Klippert, T.E., and Wozniak, D.G. (1997) The time-of-flight small–angle diffractometer at IPNS, Argonne National Laboratory. *J. Appl. Cryst.*, 30: 280–293.
23. Porod, G. (1982) General theory, Chapter 2. In *Small Angle X-Ray Scattering*. Glatter, O. and Kratky, O. (eds.); Academic Press: New York, NY, 17–51.
24. Guinier, A. and Fournet, G. (1955) *Small Angle Scattering of X-Rays*; John Wiley and Sons: New York, NY.
25. Schaekers, J.M. (1991) Extraction of inorganic acids. In *Science and Technology of Tributyl Phosphate*; Schulz, W.W., Navratil, J.D. and Kertes, A.S. (eds.), CRC Press: Boca Raton, FL; Vol. IV, 71–204.
26. Marcus, Y. and Kertes, A.S. (1969) *Ion Exchange and Solvent Extraction of Metal Complexes*; Wiley-Interscience: New York, NY.
27. Vasudeva Rao, P.R. and Kolarik, Z. (1996) A review of third phase formation in extraction of actinides by neutral organophosphorus extractants. *Solvent Extr. Ion Exch.*, 14: 955–993.
28. Chiarizia, R., Jensen, M.P., Borkowski, M., Ferraro, J.R., Thiyagarajan, P., and Littrell, K.C. (2003) SANS study of third phase formation in the U(VI), HNO_3/TBP, *n*-dodecane system. *Sep. Sci. Technol.*, 38: 3313–3331.
29. Borkowski, M., Chiarizia, R., Jensen, M.P., Ferraro, J.R., Thiyagarajan, P., and Littrell, K.C. (2003) SANS study of third phase formation in the Th(IV), HNO_3/TBP, *n*-octane system. *Sep. Sci. Technol.*, 38: 3333–3351.
30. Hiemenz, P.C. and Rajagopalan, R. (1997) *Principles of Colloid and Surface Chemistry*, Third Ed.; Marcel Dekker, Inc: New York, NY.
31. Pedersen, J.S. (1997) Analysis of small-angle scattering data from colloids and polymer solutions: modeling and least-squares fitting. *Adv. Colloid Interface Sci.*, 70: 171–210.
32. Rosen, M.J. (1989) *Surfactants and Interfacial Phenomena*, Second Ed.; Wiley-Interscience: New York, NY.